

เอกสารอ้างอิง

1. Moodera, J. S. and Mathon, G. (1999). Spin polarized tunneling in ferromagnetic junctions. **Journal of Magnetism and Magnetic Materials**, **200**, 248–273.
2. Zhu, J. and Park, C. (2006). Magnetic Tunnel Junction. **Materials today**, **9**(11), 36–45.
3. Matsugi, J., Mizoh, Y., Nakano, T., Nakamura, K., and Sakakima, H. (2005). ESD Phenomena in GMR Heads in the Manufacturing Process of HDD and GMR Heads. **IEEE Transactions on Electronics Packaging Manufacturing**, **28**(3), 206–212.
4. Chen, L., Liu, F., Stoev, K., Li, S., Ho, M. And Moa, S. (2009). Effects of pinning defects on current-perpendicular-to-plane magnetic recording heads. **Journal of Applied Physics**, **105**, 07B730 – 07B730-3.
5. Zhou, Y. (2007). Thermally Excited Low Frequency Magnetic Noise in CPP Structure MR Heads. **IEEE Transaction on Magnetic**, **43**(6), 2187–2192.
6. Han, G. C., Zong, B. Y., Luo, P., Wang, C. C. (2010). Magnetic field dependence of low frequency noise in tunnel magnetoresistance heads. **Journal of Applied Physics**, **107**(9), 09C706 – 09C706-3.
7. Han, G. C., Tan, E. L., Zong, B. Y., Zheng, Y. K., Tan, S. G. and Wang, L. (2008). Abnormal increase in ferromagnetic resonance amplitude just before the breakdown in tunnel magnetoresistive heads. **Journal of Applied Physics**, **103**, 07F518 – 07F518-3.
8. Taratorin, A. (2009). Measurement of Effective Free Layer Magnetization Orientation of TMR Sensors. **IEEE Transaction on Magnetic**, **45**(10), 3449–3452.
9. Ralph, D. C. and Stiles, M. D. (2008). Spin transfer torque. **Journal of Magnetism and Magnetic Materials**, **320**, 1190–1216.
10. Manchon, A., Ryzhanova, N., Vedyayev, A., Chschiev, M. and Dieny, B. (2009). Description of current-drive torque in magnetic tunnel junction. **Journal of Physics: Condensed Matter**, **20**, 145208 – 145208-14.
11. ทีปานิษฐ์ ชัชวาลย์. (2553). **Introduction to Electronics Structure Theory**. ขอนแก่น: ภาควิชาฟิสิกส์ คณะวิศวกรรมศาสตร์ มหาวิทยาลัยขอนแก่น.
12. Junquera, J. (2007). **Introduction to density functional theory**. Paper presented at the 1st Summer School in Theoretical and Chemistry of Catalonia, Barcelona, Spain.
13. Stefano Sanvito. (2005). Ab-initio methods for spin-transport at the nanoscale level. In Rieth, M. and Schommon, W. (Eds). **Handbook of Computational Nanotechnology Vol5**. Stevenson Ranch, CA: American Scientific.
14. Buttiker, M., Imry Y., Landauer , R., and Pinhas, S. (1985). Generalize many-channel conductance formula with application too small rings. **Physics Review B**, **31**(10), 6207–6215.

15. Rocha, A. R. (2006). **Theoretical and computational aspects of electronic transport at the nanoscale**. Ph.D. Thesis, Trinity College Dublin.
16. Runger, I. (2008). **Computation methods for electronics transport and their application in nanodevice**. Ph.D. Thesis, Trinity College Dublin.
17. Datta, S. (2004). Electrical resistance: an atomic view. **Nanotechnology**, **15**, S433–S451.
18. Supriyo Datta. (1995). **Electronics transport in mesoscopic systems**. Cambridge: Cambridge University Press.
19. Supriyo Datta. (2005). **Quantum transport: Atom to transistor**. Cambridge: Cambridge University Press.
20. Massimiliano Di Ventra. (2008), **Electrical transport in nanoscale systems**. Cambridge: Cambridge University Press.
21. Rungger, I. and Sanvito, S. (2008). Algorithm for the construction of self-energies for electronic transport calculations based on singularity elimination and singular value decomposition. **Physics Review B**, **78**, 035407 – 035407–13.
22. Rungger, I. (2009). **Quantitative theory for electron transport in nanodevice**. Paper presented at Summer School on modeling nanostructure using density functional theory, Izmir, Turkey.
23. Moodera, J., Santos, T. S. and Nagahama, T. (2007). The Phenomenal of spin-filter tunneling. **Journal of Physics: Condensed Matter**, **19**, 165202 – 165202–12.
24. Schmidt, G. (2005). Concept for spin injection into semiconductors—a review. **Journal of Physics D: Applied Physics**, **38**, R107–R122.
25. Pertsev, N. A. and Kohlstedt, H. (2009). Magnetic tunnel junction on a ferroelectric substrate. **Applied Physics Letter**, **95**, 163503 – 163503–3.
26. Tsymbal, E. Y., Mryasov, O. N. and LeClair, P. R. (2003). Spin-dependent tunneling in magnetic tunnel Junction. **Journal of Physics: Condensed Matter**, **15**, R109– R142.
27. Miyazaki, T. and Tezuka, N. (1995). Giant magnetic tunneling effect in Fe/Al₂O₃/Fe junction. **Journal of Magnetism and Magnetic Materials**, **139**, L231–L234.
28. Moodera, J. S., Kinder, Lisa R., Wong, Terrilyn M., and Meservey, R. (1995). Large magnetoresistance at room temperature in ferromagnetic thin film tunnel junctions. **Physics Review Letters**, **74**(16), 3273–3276.
29. Butler, W. H., Zhang, X.-G., Schulthess, T. C., MacLaren, J. M. (2001). Spin-dependent tunneling conductance of Fe/MgO/Fe sandwiches. **Physical Review B**, **63**, 054416 – 054416–12.
30. Parkin, S. S. P., Kaiser, C., Panchula, R., Rice, P.M., Hughes, B., Samant, M. et al. (2004). Giant tunneling magnetoresistance at room temperature with MgO (100) tunnel barriers. **Nature Material**, **3**, 862–867.
31. Yuasa, S., Nagahama, T., Fukushima, A., Suzuki, Y. and Ando, K. (2004). Giant room-temperature magnetoresistance in single-crystal Fe/MgO/Fe magnetic junction. **Nature Material**, **3**, 868–871.

32. Djayaprawira, D., Tsunekawa, K., Nagai, M., Machara, H., Yamagata, S., Watanabe, N., et al. (2005). 230% room-temperature magnetoresistance in CoFeB/MgO/CoFeB magnetic tunnel junctions. **Applied Physics Letters**, **86**, 092502 –092502–3.
33. Mao, S., Nowak, J., Song, D., Kolbo, P., Wang, L., Linville, E., et al. (2002). Spin tunneling head above 20 Gb/in² and beyond. **IEEE Transaction on Magnetic**, **38**(1), 78–83.
34. Mao, S., Linville, E., Nowak, J., Zhang, Z., Chen, S., Karr, B., et al. (2004). Tunneling magnetoresistive head beyond 150 Gb/in². **IEEE Transaction on Magnetic**, **40**(1), 307–312.
35. Mao, S., Chen, Y., Liu, F., Chen, X., Xu, B., Lu, P., et al. (2006). Commercial TMR heads for hard disk drives: Characterization and extendibility at 300 Gbit/in². **IEEE Transaction on Magnetic**, **42**(2), 97–102.
36. Yuasa, S. and Djayaprawira, D. (2007). Giant tunneling magnetoresistance in magnetic tunnel junction with a crystalline MgO (001) barrier. **Journal of Physics D: Applied Physics**, **40**, R337–R354.
37. Julliere, M. (1975). Tunneling between ferromagnetic films. **Physics Letters A**, **54**(3), 225–226.
38. Naber, W. M. (2010). **Electron transport and spin phenomena in hybrid organics/inorganic**. PhD. Thesis, University of Twente.
39. Parkin, S., Yang, S., Yang, S.H. and Hayashi, M. (2007). **Magnetic Tunneling Junction**. Hand book of Magnetism and advance magnetic materials, 5 John Wiley & Son , 2571–2591.
40. S. X. Huang, T. Y. Chen, and C. L. Chien (2008). Spin polarization of amorphous CoFeB determined by point-contact Andreev reflection. **Applied Physics Letter**, **92**, 242509 –242509–3.
41. Butter, W. H. (2008). Tunneling magnetoresistance from a symmetry filter effect. **Science and Technology of Advanced Materials**, **9**, 014106 – 014106–17.
42. Tiusan, C., Greullet, F., Hehn, M., Montaigne, F., Andrieu, S. and Schuhl, A. (2007). Spin tunneling phenomena in single-crystal magnetic tunneling junction systems. **Journal of Physics: Condensed Matter**, **19**, 165201– 165201–35.
43. Reiss, G., Schmalhorst, J., Thomas, A., Hütten, A. And Yuasa, S. (2008). Magnetic tunneling junction. In G. Holer (Eds). **Springer trace in modern physics**. (pp. 291–333). NY: Springer.
44. Oliver, B., Tuttle, G., He, Q., Tang, X. and Nowak, J. (2004). Two breakdown mechanism in ultrathin alumina barrier magnetic tunnel junctions. **Journal of Applied Physics**, **95**(3), 1315–1322.
45. Khan, A., Schmalhorst, J., Thomas, A., Schebaum, O. and Reiss, G. (2008). Dielectric breakdown in Co–Fe–B/MgO/Co–Fe–B magnetic tunnel junction. **Journal of Applied Physics**, **103**, 123705 – 123705–5.

46. Velez, J. P., Belashchenko, K. D., Jaswal, S. S. and Tsymbal, E. Y. (2007). Effect of oxygen vacancies on spin-dependent tunneling in Fe/MgO/Fe magnetic tunnel junctions. **Applied Physics Letters**, **90**, 072502 – 072502-3.
47. Xi, H., Franzen, S., Guzman, I. And Moa, S. (2007). Degradation of magnetic tunneling junctions caused by pinhole formation and growth. **Journal of Magnetism and Magnetic Materials**, **319**, 60–63.
48. Thomas, A., Drewello, V., Schafers, M., Weddemann, A., Reiss, G., Eilers, G., et al. (2008). Direct imaging of the structural change generated by dielectric breakdown in MgO based magnetic tunnel junctions. **Applied Physics Letter**, **93**, 152508 –152508-3.
49. Dimitrov, D. V., Gao, Z., Wang, X., Jung, W., Lou, X. And Heinonen, O. G. (2009). Dielectric breakdown of MgO magnetic tunnel junctions. **Applied Physics Letter**, **94**, 123110 – 123110-3.
50. Victora, R.H. and Chen, X. (2010). Predicted effects of pinhole and surface roughness in magnetoresistive read head. **IEEE Transaction on Magnetic**, **46**(3), 702–708.
51. Kanu G.Ashar. (1997). **Magnetic Disk Drive Technology: Heads, Media, Channel, Interfaces, and Integration**. New York: IEEE Press.
52. Khizroev, S. and Litvinov, D. (2004). Perpendicular magnetic recording: writing process. **Journal of Applied Physics**, **95**(9), 4521–4537.
53. Gao, K.Z., Heinonen, O., and Chen, Y. (2008). Read and write process, and head technology for perpendicular recording. **Journal of Magnetism and Magnetic Materials**, **321**, 495–507.
54. Kiyono, H., Hachisuka, N., Saruki, S. and Kasahara, N. (2007). Composite Type Thin Film Magnetic Head having a Low Parasitic Capacitance between a Write Coil and an Upper Read Head Shield. **United State Patent**, 7274539B.
55. Sining Mao. (2004). Tunneling Magnetoresistive head in current perpendicular to plane mode. **United State Patent**, 6700760 B1.
56. Inage, K., Saruki, S. and Hachisuka, N. (2006). Thin film magnetic head with tunnel magnetoresistive effect element electrically connected in Parallel with a resistance element. **United State Patent**, 7102859 B2.
57. Leung, E. C. W., Lai, A. W. Y., Won, P. K., Hu, D., Dovek, M. and Lee, R. (2008). ESD, Crosstalk and Noise Pickup Minimizing Scheme for CPP and TMR Device. **United State Patent**, 0259506 A1.
58. Mao, S., Nowak, J., Linville, E. S., Chen, H. S. S. and Xue, S. S. (2006). TMR Head Structure with Conductive Shunt. **United State Patent**, 7151654 B1.
59. Shang, C., Li, Y. S., Hu, Y. and Shen, Y. (2008). Method to Fabricate an ESD Resistant Tunneling Magnetoresistive Read Transducer. **United State Patent**, 7389577 B1.
60. Chen, Y. J. and Larson, D. B. (2009). Head gimbal assembly including a flexure with first conductive trace disposed between a slider and a dielectric layer. **United State Patent**, 7595965 B1.

61. Electrostatic Discharge Association. (2003). **Test Method for electrostatic discharge sensitivity testing–Human Body Model Component Level**. USA: Electrostatic Discharge Association.
62. JEDEC Solid State Technology Association. (2006). **Electrostatic sensitive testing human body model**. USA: JEDEC Solid State Technology Association.
63. Coca, E. and Buta, G. (2008). **A review of ESD stress model**. Paper presented at 9th International Conference on Development and application system, Suceava, Romania.
64. Electrostatic Discharge Association. (2001). **Test Method for electrostatic discharge sensitivity testing – Machine Model Component Level**. USA: Electrostatic Discharge Association.
65. Electrostatic Discharge Association. (2001). **Test Method for electrostatic discharge sensitivity testing – Charged Device Model Component Level**. USA: Electrostatic Discharge Association.
66. Guarisco, D. (2008). Resilience of tunneling magnetoresistive heads against electrical overstress. **Journal of Applied Physics**, **103**, 07F535 – 07F535–3.
67. Feng, L., Chang, C.H. and Jian, S. and Pant, B.B. (2006). Characteristic of Electrostatic Discharge Induce Damage on Magnetic Tunneling Junctions. **IEEE Transaction on Magnetic**, **42(10)**, 2447–2449.

ภาคผนวก

การเผยแพร่ผลงานวิทยานิพนธ์

1. Jutong, N., Somponges, D., Rakpongsiri, P. and Siritaratiwat, A. (2009). Dependence of Flex on suspension capacitance on human-body-model-electrostatic-discharge affected TMR read head. **Solid State Phenomena**, **152-153**, 439-442.
2. Jutong, N., Siritaratiwat, A., Somponges, D. and Rakpongsiri, P. (2009). Electrostatic discharge effect on TMR recording head: A flex on suspension capacitance approach. **International Journal of Modern Physics B**, **23(17)**, 3586-3590.
3. Jutong, N., Somponges, D. and Siritaratiwat, A. (2010). Dependence of discharge path on breakdown characteristic of tunneling magnetoresistive read heads. **Journal of Electrostatics**, Accept on 22 June

DEPENDENCE OF FLEX ON SUSPENSION CAPACITANCE ON HUMAN-BODY- MODEL- ELECTROSTATIC- DISCHARGE AFFECTED TMR HEAD

N. Jutong^{1,a}, D. Sompongse^{2,b}, P. Rakpongsiri^{2,c} and A. Siritaratiwat^{1,d}

¹ Department of Electrical Engineering, Khon Kaen University, Khon Kaen, 40002, THAILAND

² Western Digital (Thailand) Co., Ltd., BangPa-In Industrial Estate, Ayutthaya, 13160, THAILAND

^a4870400074@stdmail.kku.ac.th, ^bduangporn.sompongse@wdc.com,

^cpornchai.rakpongsiri@wdc.com, ^dapirat@kku.ac.th

Keywords: FOS capacitance, Electrostatic discharge, TMR head

Abstract. Electrostatic discharge (ESD) effects on GMR recording heads have been reported as the major cause of head failure. Since the information density in hard-disk drives has dramatically increased, the GMR head will be no longer used. The tunneling magnetoresistive (TMR) read heads are initially introduced for a 100 Gbit/in² density or more. Although the failure mechanism of ESD in GMR recording head has not been explicitly understood in detail, study to protect from this effect has to be undergone. As the TMR head has been commercially started, the ESD effect is closely watched. This is the first time report of the TMR equivalent circuit in order to evaluate the ESD effect. A standard human body model (HBM) is discharged across R+ and R- where the capacitance of flex on suspension (FOS) is varied. It is intriguingly found that the electrical characteristic of the TMR head during discharge period depends on discharge position. This may be explained in terms of asymmetry impedance of TMR by using adapted Thevenin's theory. The effect of FOS component on TMR recording head is also discussed.

Introduction

Tunneling Magnetoresistive (TMR) read heads are used for data storage density higher than 100 Gbit/in² in magnetic recording heads [1]. The structure of a TMR head is considerably different from GMR head. TMR sensors uses ultra-thin insulator barrier and are subjected to bias current perpendicularly [2], whereas a GMR head bias current is longitudinal. It is a symmetry circuit [3]. Therefore, the effect of ESD on a TMR head is different from GMR head [4]. The equivalent circuit model of a GMR head is widely used to understand behavior of GMR heads upon ESD in the Head Gimbal Assembly (HGA) and Hard Disk Drive Assembly (HDA) [5]. However, an equivalent circuit of a TMR head remains unexplored. This study presents, for the first time, the TMR equivalent circuit in order to evaluate ESD effect on TMR recording head.

Equivalent Circuit Model of TMR Head

The equivalent circuit of a TMR read head at HGA-level for a hard disk drive with aerial density of 100-160 Gbit/in² consists of 4 major parts, as described in Fig. 1: Part 1 Read element, Part 2 Shunting element, Part 3 FOS+ - FOS-, and Part 4 Suspension.

In Part 1, the TMR read head includes top shield, bottom shield, substrate, insulator layer and TMR sensor. Both top and bottom shields are magnetically shielded and they also act as electrodes for sensing current perpendicularly to the surface of the TMR sensor [2]. An electrical insulator is filled in the gap between top-bottom shields or the shield-shield gap (SS gap). These top shield, bottom shield, SS gap and TMR sensors are placed on a substrate. In the gap between bottom shield and substrate (BS gap) an electrical insulator is also inserted. An electrical circuit for this head structure can be developed by using a parallel-plate-capacitance model.

In Part 2, since the TMR sensor is currently considered as the most ESD sensitive device, the technique of shunting resistance is employed to protect the head from ESD transient voltage.

A Flex on Suspension (FOS), in Part 3, is used for sensing current to read head in between top and bottom shields. It can be modeled as a T-type-transmission-line with an RLC circuit. These 3 parts are then placed on a suspension, Part 4, by using insulating adhesive. Therefore, a parallel-plate capacitance and a resistance can be considered as an electrical interconnection model between substrate and suspension.

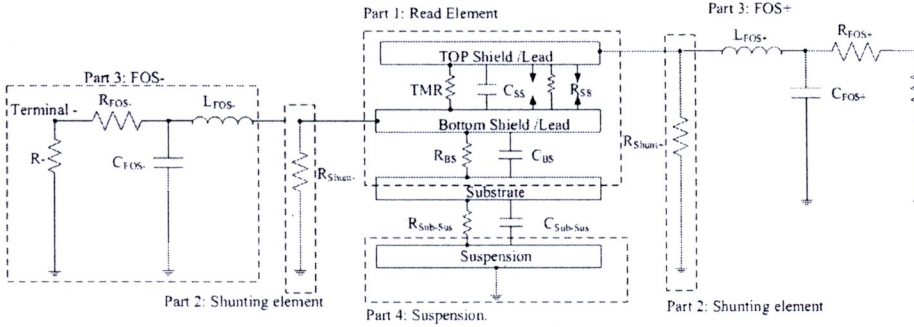


Fig. 1 Equivalent circuit of TMR recording head at HGA-level.

Experiment Result and Discussion

Because the current flow into a TMR sensor (I_{TMR}) can not be directly measured in real magnetic recording head. An equivalent circuit is used to study ESD effect in TMR heads. The standard Human Body Model (HBM) is employed for ESD study discharging across R^+ and R^- terminals. An ESD voltage (V_{ESD}) is varied until I_{TMR} is larger than 1.25 mA. This amount of current is set by manufacturing criteria for head degradation awareness.

Since FOS+ and FOS- are typically symmetric, a study of FOS capacitance effect on TMR head at varied applied voltage is done.

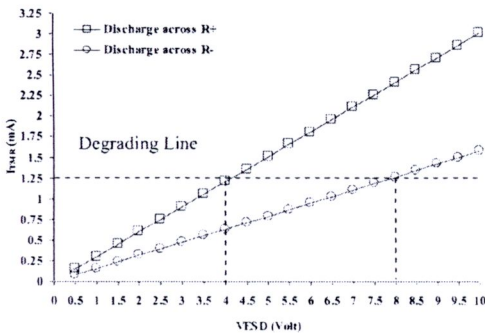


Fig. 2 Dependence of V_{ESD} on discharge terminal

It is clearly seen from Fig. 2 that I_{TMR} is doubly sensitive to V_{ESD} for R^+ discharging rather than that for R^- discharging. The least magnitudes of V_{ESD} required to degrade TMR head are ~ 4 V and ~ 8 V for R^+ and R^- discharging respectively. This result must be seriously taken into account because it implies that the total impedance of TMR (Z_{TMR}) when discharging across R^- is higher than that when discharging across R^+ . Since R^+ , R^- , R_{BS} and $R_{Sub-Sus}$ are normally larger than 1,000 M Ω , they are assumed to be open circuits, as shown in Fig. 3. This TMR equivalent circuit is firstly

proposed in order to calculate $Z(j\omega)$ as well as to evaluate the relationship between $I_{TMR}(j\omega)$ and circuit elements by using an adapted Thevenin's theory.

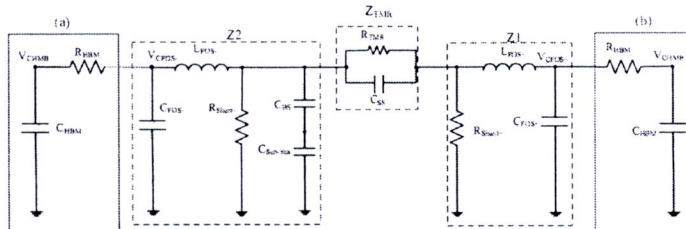


Fig. 3 TMR equivalent circuit for discharging across (a) R- and (b) R+.

The total impedances, Z_{TMR} or $Z(j\omega)$, for discharging across R+ and R- are approximately given by

$$Z_{TMR}^+(j\omega) \approx \frac{1}{G_{TMR}^+(j\omega)} \quad (1)$$

$$Z_{TMR}^-(j\omega) \approx \frac{1}{G_{TMR}^-(j\omega)} \quad (2)$$

where $G_{TMR}^+(j\omega)$ and $G_{TMR}^-(j\omega)$ are total frequency-dependent TMR admittances when discharging across R+ and R- respectively.

The V_{ESD} of 2 different discharging positions are now considered in the frequency domain. Therefore, the calculation in Eq. 1 and Eq. 2 must be under conditions that

$$V_{ESD}^+(j\omega) = V_{C_{ESD}}(0) - V_{C_{ESD}}(j\omega) \quad (3)$$

$$V_{ESD}^-(j\omega) = V_{C_{ESD}}(0) - V_{C_{ESD}}(j\omega) \quad (4)$$

From Eq. 1 and Eq. 2, it must be kept in mind that the dependence of $1/G_{TMR}(j\omega)$ on frequency is in the same sense as that of $Z_{TMR}(j\omega)$ and this relationship is shown in Fig. 4. It is obviously confirmed by asymmetric TMR impedance that $1/G_{TMR}^-(j\omega) > 1/G_{TMR}^+(j\omega)$ and so, $Z_{TMR}^-(j\omega) > Z_{TMR}^+(j\omega)$ as mentioned.

The relationship between $I_{TMR}(j\omega)$ and circuit elements can be calculated by multiplying V_{ESD} by Eq. 1 and Eq. 2. Therefore $I_{TMR}(j\omega)$, for R+ and R- discharging, is inversely proportional to $G_{TMR}^+(j\omega)$ and $G_{TMR}^-(j\omega)$ respectively. The $G_{TMR}^+(j\omega)$ and $G_{TMR}^-(j\omega)$ are more conveniently analyzed by using Laplace's transform technique than a direct frequency domain solving technique, as given in Eq. 5 and Eq. 6.

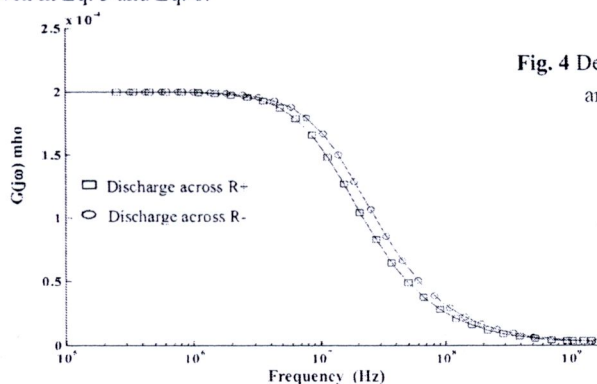


Fig. 4 Dependence of $1/G(j\omega)$ for R+ and R- discharging.

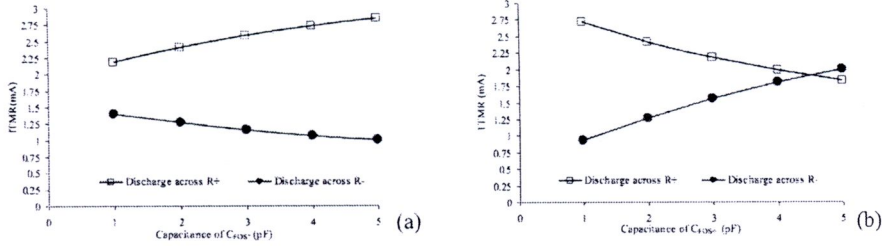


Fig. 5 Dependence of I_{TMR} on (a) C_{FOS-} and (b) C_{FOS+} .

$$G_{TMR}^+(j\omega) = R_{shunt+} \times [(j\omega R_{shunt-} C_x + 1)((j\omega)^2 L_{FOS-} C_{FOS-} + 1) + (j\omega R_{shunt-} C_{FOS-})] \quad (5)$$

$$G_{TMR}^-(j\omega) = R_{shunt-} \times [(1 + j\omega R_{shunt+} C_{FOS+} + (j\omega)^2 R_{FOS+} C_{FOS+})] \quad (6)$$

where $C_x = C_{BS} // C_{sub-stub}$

It is observed that $G_{TMR}^+(j\omega)$ and $G_{TMR}^-(j\omega)$ depend on C_{FOS-} and C_{FOS+} respectively. Thus, the dependences of I_{TMR} on C_{FOS-} and C_{FOS+} , as discharging R+ and R-, are shown in Fig. 5. It is seen from Fig. 5 (a) when C_{FOS-} increases that I_{TMR} proportionally increases with C_{FOS-} for R+ discharging but decreases for R- discharging. Intriguingly, I_{TMR} exhibits the opposite when C_{FOS+} increases, as shown in Fig. 5 (b). From this result, it is found that TMR head is dependent on both FOS capacitance and ESD discharging position. This is evidently attributed to an asymmetric circuit for the TMR head. Therefore, current conventional ESD detections in GMR head are definitely unable to serve in TMR head manufacturing and methodology for ESD capturing will be complicated to investigate.

Summary

It is initially found that impedance of TMR recording head is asymmetric by using information of current manufactured TMR heads. It is undoubtedly shown that degradation of TMR head depends on ESD discharging position (R+ / R-) and FOS capacitance (C_{FOS-} / C_{FOS+}). The equivalent circuit of an asymmetric TMR head is also proposed for the first time. From this result, it is noticed that present ESD detection in manufacturing is no longer sufficient and a novel complex measurement has to be further invented for detecting ESD in TMR recording heads.

Acknowledgement

This research is funded by the I/U CRC in HDD Components, Khon Kaen University, and the National Electronics and Computer Technology Center (NECTEC) under the National Sciences and Technology Development Agency (NSTDA), Thailand, Grant No. CPN-HR-03-10-50 D. Authors would like to dedicate this work to staff of Western Digital (BangPa-In), Thailand, for their provision of samples, facilities and technical discussion.

References

- [1] S. Mao et al: IEEE Trans. Magn. Vol. 40 (2004), p. 307.
- [2] K. Inage, US Patent 7,102,859 B2. (2006)
- [3] A. Siritaratiwat et al: J.Magn.Mag.Mater. Vol. 272-276 (2004), p.2307.
- [4] F. Liu et al: IEEE Trans. Magn. Vol. 42 (2006), p.2447
- [5] Al Wallash: J. Micro Relia. Vol. 45 (2005), p. 305

Magnetism and Magnetic Materials

doi:10.4028/3-908454-13-1

Dependence of Flex on Suspension Capacitance on Human-Body-Model-Electrostatic-Discharge Affected TMR Head

doi:10.4028/3-908454-13-1.439



ELECTROSTATIC DISCHARGE EFFECT ON TMR RECORDING HEAD: A FLEX ON SUSPENSION CAPACITANCE APPROACH

NUTTACHAI JUTONG^a and APIRAT SIRITARATIWAT^{b*}

Department of Electrical Engineering, Khon Kaen University,

Khon Kaen, 40002, Thailand

^a4870400074@kku.ac.th

^{b*}apirat@kku.ac.th

DUANGPORN SOMPONGSE^c and PORNCHAI RAKPONGSIRI^d

Western Digital (Thailand) Co., Ltd., BangPa-In Industrial Estate,

Ayutthaya, 13160, Thailand

^cduangporn.sompongse@wdc.com

^dpornchai.rakpongsiri@wdc.com

Received 30 September 2008

Electrostatic discharge (ESD) effects on GMR recording heads have been reported as the major cause of head failure. Since the information density in hard-disk drives has dramatically increased, the GMR head will be no longer in use. The tunneling magnetoresistive (TMR) read heads are initially introduced for a 100 Gbit/in² density or more. Though the failure mechanism of ESD in GMR recording heads has not been explicitly understood in detail, a study to protect from this effect has to be done. As the TMR head has been commercially started, the ESD effect must be considered. This is the first time that the TMR equivalent circuit has been reported in order to evaluate the ESD effect. A standard human body model (HBM) is discharged across R+ and R- where the capacitances of flex on suspension (FOS) are varied. It is intriguingly found that the electrical characteristics of the TMR head during the discharge period depend on the discharge position. This may be explained in terms of the asymmetry impedance of TMR by using adapted Thevenin's theory. The effect of FOS components on TMR recording heads is also discussed.

Keywords: Electrostatic Discharge; TMR Recording Head; FOS Capacitance; Equivalent Circuit Model

1. Introduction

Tunneling Magnetoresistive (TMR) read heads are promising for ultra high density HDD¹. A high MR ratio of TMR sensor results in an ultra thin insulator barrier¹. It is thought to be the root cause of failure in TMR heads. The failure threshold of TMR readers against electrostatic discharge (ESD) is generally lower than that for GMR sensors². ESD characteristics induce TMR degradation differently from a conventional GMR recording head³. The equivalent circuit model of a GMR head is widely used to understand the behavior of GMR heads upon ESD in processes of Head Gimbal Assembly (HGA), Head Stack Assembly (HSA) or Hard Disk Drive Assembly (HDDA)⁴. However, an equivalent circuit model of the TMR head remains unexplored. This study presents for the first time an equivalent circuit model in order to evaluate the ESD effect on TMR recording heads.

2. Equivalent Circuit of TMR Recording Head

In Fig. 1, it shows the equivalent circuit of a TMR read head at the HGA-level that consists of 4 parts; Part 1 (read element), Part 2 (shunting element), Part 3 (FOS+ and FOS-) and Part 4 (suspension).

It is seen that insulated top-bottom shields are considerably in parallel plate capacitance form and represented by C_{SS} parallel with R_{SS} . In the same manner, the gaps of bottom-shield-to-substrate (BS gap) and substrate-to-suspension (SS gap) are represented by C_{BS} parallel with R_{BS} and $C_{Sub-Sus}$ parallel with $R_{Sub-Sus}$ respectively. The shunted resistance of top-shield-to-ground and bottom-shield-to-ground are represented by R_{Shunt+} and R_{Shunt-} respectively. "Type T" transmission line equivalent circuit model is used to represent flex on suspension, FOS, which is connected between terminal +(-) and bottom (top) shield, are represented by $R_{FOS+(-)}$, $C_{FOS+(-)}$ and $L_{FOS+(-)}$ respectively. Terminal + (-) are represented by $R_{FOS+(-)}$. The TMR sensor which is placed vertically between top and bottom shield is represented by R_{TMR} .

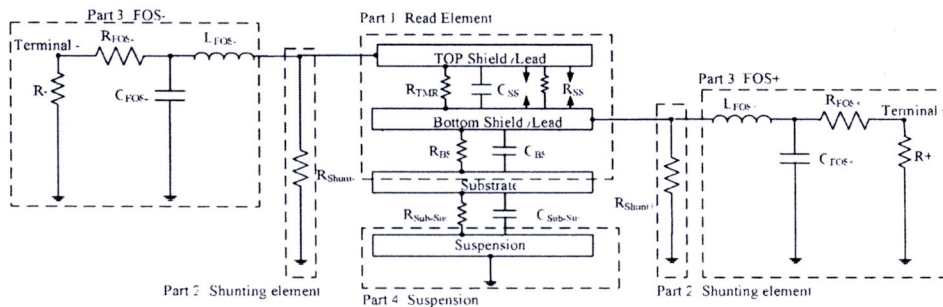


Fig. 1. Equivalent circuit model of TMR read head at HGA-level.



3. Experiment Results and Discussion

The ESD effect based on Human Body Model (HBM) is studied in two cases;

- condition 1 = discharging across R+ and
- condition 2 = discharge across R- .

In each case, the ESD voltage (V_{ESD}) was varied in each value of FOS capacitance (C_{FOS+} and C_{FOS-}) and the current flow measured into R_{TMR} until the head degraded. A peak current induced in this TMR sensor model will be degraded at about 1.25 mA. The V_{ESD} that induces head degradation is called the breakdown voltage ($V_{Breakdown}$).

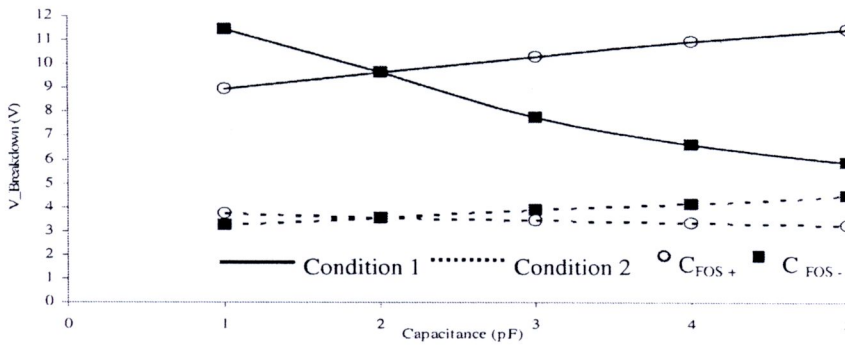


Fig. 2. Dependence of FOS capacitance on $V_{Breakdown}$.

The ESD effect on TMR recording heads was studied by using the equivalent circuit model in Fig. 1. It is seen from Fig. 2 that breakdown voltages required for condition 2 are lower than that for condition 1 at the same value of C_{FOS+} and C_{FOS-} . An increase of C_{FOS+} causes voltage breakdown for both conditions 1 and 2 where the breakdown voltages tend to increase dramatically for the first condition and decrease slightly for the other. On the other hand, when C_{FOS-} increases the breakdown voltages tend to decrease dramatically for condition 1 and increase slightly for condition 2.

For condition 1, it is seen from Figs. 2 and 3 that a current flowing into R_{TMR} varies with C_{FOS-} but inversely varies with C_{FOS+} . On the contrary, for condition 2, a current flowing into R_{TMR} varies with C_{FOS+} but inversely varies with C_{FOS-} . These results can be proved by using an adapted Thevenin equivalent circuit.

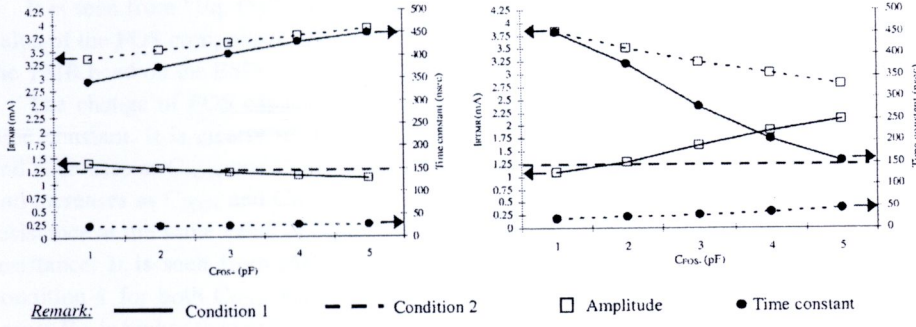


Fig. 3. Dependence of FOS capacitance on amplitude and time constant at $V_{ESD}=10$ V for (a) C_{FOS+} and (b) C_{FOS-} .

Current flowing into R_{TMR} in the frequency domain for both conditions are given by

$$I_{TMR}^+(j\omega) \approx V_{ESD}^+(j\omega)G_{TMR}^+(j\omega) \quad (1)$$

$$I_{TMR}^-(j\omega) \approx V_{ESD}^-(j\omega)G_{TMR}^-(j\omega) \quad (2)$$

The V_{ESD} in the frequency domain of both sides are given by

$$V_{ESD}^+(j\omega) = V_{C_{HBM}}(0) - V_{C_{FOS+}}(j\omega) \quad (3)$$

$$V_{ESD}^-(j\omega) = V_{C_{HBM}}(0) - V_{C_{FOS-}}(j\omega) \quad (4)$$

where

$$G_{TMR}^+(j\omega) = R_{shunt+} \times [(1 + sR_{shunt+}C_{FOS-} + s^2R_{FOS-}C_{FOS-})] \quad (5)$$

$$G_{TMR}^-(j\omega) = R_{shunt-} \times [(sR_{shunt+}C_x + 1)(s^2L_{FOS+}C_{FOS+} + 1) + (sR_{shunt+}C_{FOS+})] \quad (6)$$

$$C_x = C_{BS} // C_{sub-sus} \quad (7)$$

At the same value of $V_{ESD}^+(j\omega)$ and $V_{ESD}^-(j\omega)$, "Eq. (1)" and "Eq. (2)", can be arranged as

$$I_{TMR}^+(j\omega) \approx \frac{1}{G_{TMR}^-(j\omega)} \quad (8)$$

$$I_{TMR}^-(j\omega) \approx \frac{1}{G_{TMR}^+(j\omega)} \quad (9)$$

It is seen from “Eq. (5)” and “Eq. (6)” that $G_{TMR}^+(j\omega)$ and $G_{TMR}^-(j\omega)$ vary with the value of the FOS component. This indicates that the value of the FOS capacitance affects the TMR head on the ESD.

The change of FOS capacitance affects not only to the TMR current but also to the time constant. It is clearly seen in Fig. 3 that, for condition 1, it dramatically increases and decreases as C_{FOS+} and C_{FOS-} increase. However, for condition 2, it slightly decreases and increases as C_{FOS+} and C_{FOS-} increase. Generally, the time constant is proportional to resistance at the same value of capacitance. Thus, a slow time constant is given by a high resistance. It is seen from Fig. 3 that the time constant of condition 2 is slower than condition 1 for both C_{FOS+} and C_{FOS-} . Approximately, the total impedance of discharge across R+ is higher than across R-.

4. Summary

It has been found that breakdown voltage of a TMR head is dependent on discharge terminal. The R- discharging is seen to be more sensitive to ESD than the R+ discharging. The TMR current is also noted to be dependent on the value of the FOS component. It has also been seen that the slow time constant of the TMR head may be robust to ESD. This result must be considered in the process of TMR design for ESD protection.

Acknowledgments

This research is funded by the Industry/University Cooperative Research Center in HDD Component, Khon Kaen University, and the National Electronics and Computer Technology Center (NECTEC) under the National Sciences and Technology Development Agency (NSTDA), Thailand, Grant No. CPN-HR-03-10-50 D. Authors would like to dedicate this work to staff of Western Digital (BangPa-In), Thailand, for their provision of samples, facilities and technical discussion.

References

1. S. Mao et al, *IEEE Trans. Magn.* **40**, 307 (2004).
2. D. Guarisco, *J. Appl. Phys.* **103**, 07F535 (2008).
3. F. Liu et al, *IEEE Trans. Magn.* **42**, 2447 (2006).
4. A. Siritaratiwat et al, *J. Magn. Mag. Mater.* **272-276**, 2307 (2004).



Dependence of discharge path on breakdown characteristic of tunneling magnetoresistive read heads

N. Jutong^a, D. Sompongse^b, A. Siritaratiwat^{a,*}

^a Department of Electrical Engineering, Khon Kaen University, 123, Friendship Road, Khon Kaen 40002, Thailand

^b Western Digital (Thailand) Co., Ltd., Ayutthaya, 13160, Thailand

ARTICLE INFO

Article history:

Received 5 December 2009

Received in revised form

14 June 2010

Accepted 22 June 2010

Available online xxx

Keywords:

Electrostatic discharge

Breakdown characteristic

Tunneling magnetoresistive read head

ABSTRACT

The dependence of discharge path on the breakdown of a TMR head was performed by using human body model in 4 cases: R+ → R− (1st), R− → R+ (2nd), R− → ground (3rd) and R+ → ground (4th). It is seen by using the TMR read head equivalent circuit that, at first, the 1st and 3rd, and the 2nd and 4th, cases present an intrinsic and extrinsic breakdown, respectively. A potential difference across the substrate is thought to cause a different breakdown mechanism. Dependence of voltage polarity across the TMR sensor on asymmetry parameter is also discussed.

© 2010 Elsevier B.V. All rights reserved.

1. Introduction

AT PRESENT, DATA storage technologies based on tunneling magnetoresistive (TMR) read heads are used in ultra high storage magnetic hard disk drives for a density greater than 200 Gb/in² [1–3]. Electrostatic discharge (ESD) affecting the TMR read head characteristic differs from that of giant magnetoresistive read heads [2,3]. Recently, it has been found that the equivalent circuit, based on ESD study, of the TMR read head is asymmetric [4, 6–8]. The discharging across the R+ terminal and ground is more robust than that across R− and ground. Since this study primarily presents the difference of both simulated circuits, details of TMR read head degradation have not been explicitly disclosed. Investigation of TMR read head breakdown characteristic when discharging along different paths is first presented in this study.

2. Experiment

2.1. Experimental method

The Standard Human Body Model (HBM) consisting of a 100 pF capacitor and a 1500 Ω resistor is used as the ESD discharge source. A set of 40 current perpendicular-recording-heads with a 160 Gb/in²

areal density TMR read head placed on Head Gimbal Assembly (HGA) were separated into 4 cases of study. Each quarter of these samples was used to study the TMR breakdown characteristics:

- 1st case = discharging from R+ to R− terminals,
- 2nd case = discharging from R− to R+ terminals,
- 3rd case = discharging from R+ to ground and
- 4th case = discharging from R− to ground.

In order to simulate an ESD event affecting the read head in each case, the ESD voltage was varied with different conditions. For the 1st and 2nd cases, the ESD voltage was increased in steps of 0.5 V, whereas, for the other cases, the ESD voltage was adjusted in steps of 1 V. The resistance, amplitude and asymmetry of the TMR read head were measured by using a Quasi Static tester (QST) after the ESD voltage was applied. The ESD voltage for each case was varied until a resistance change of the order of 20% was observed. This percentile value of resistance change, called the point of “breakdown voltage”, was typically set in manufacturing for head failure awareness.

2.2. Simulation method

An equivalent circuit model of a TMR read head was ultimately developed for breakdown mechanism analysis [2]. The circuit model of a 200 Gb/in² TMR read head consists of 4 parts, as show in Fig. 1:

* Corresponding author.

E-mail address: apirat@kku.ac.th (A. Siritaratiwat).

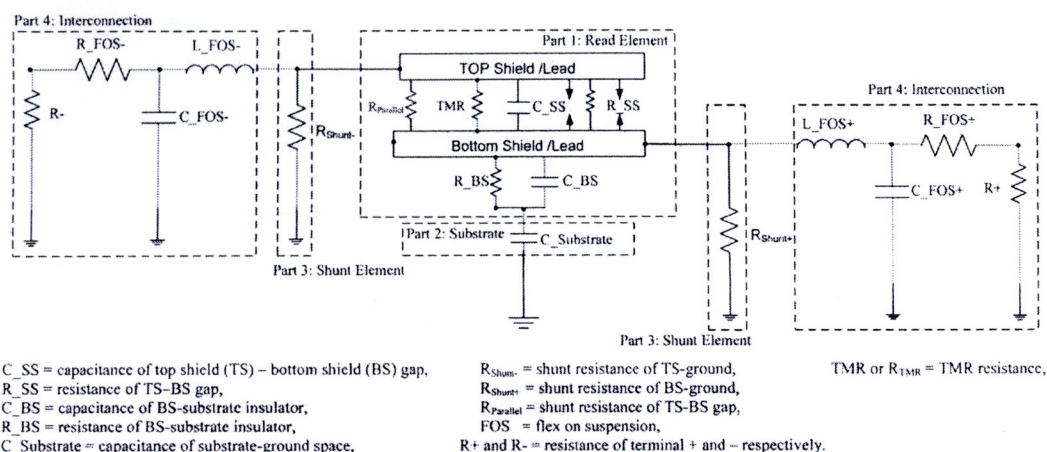


Fig. 1. Equivalent circuit of TMR read head.

- Part 1 = Read element,
- Part 2 = Shunting element,
- Part 3 = FOS+ and FOS–, and,
- Part 4 = Suspension.

The standard HBM is employed for breakdown study for each case and the schematic diagrams are shown in Fig. 2. The simulation procedure is started by applying an ESD voltage to C_{HBM} and then measuring the voltage across TMR and $C_{Substrate}$. During discharge, static energy can be stored in terms of capacitance around the sensor, especially the capacitance between substrate and ground ($C_{Substrate}$). This activated energy can accelerate the breakdown [9]. Therefore, in order to study the breakdown characteristic, the voltage across $C_{Substrate}$ must be measured.

3. Results and discussions

In general, the breakdowns of TMR read head are classified into 2 types, intrinsic and extrinsic breakdowns, by observing the resistance changes. The intrinsic breakdown shows an abrupt resistance change whereas the extrinsic one is recognized when the resistance changes gradually [5,9,10].

The intrinsic breakdown is easily explainable using the electric field model, E-Model. This is because when a dielectric material is subjected to an electric field, the net dipole moment is then induced and bond distorted [9]. In the E-Model study, the arisen energy can accelerate the probability of dielectric breakdown and so, it is called the activation energy, E_A . The E_A is an energy required for ion jumping over a distance of an atomic space in the direction of the electric field decrement [11].

The extrinsic breakdown results in joule heating by inducing pinhole or nanocontact of ferromagnetic layers across the insulator barrier. Two kinds of extrinsic breakdown occur by power dissipation generated from current perpendicular to the TMR at beyond critical voltage and are in the form of the appearance of other pinholes in the barrier and the expansion of existing pinholes in the barrier [12].

The dependence of ESD discharging path is demonstrated based on these two breakdown characteristics using static test parameters; resistance and asymmetry.

3.1. Resistance measurement

ESD can cause both intrinsic and extrinsic breakdowns in a TMR read head. The resistances changes when varying the ESD are measurement on take four different discharging paths as shown in Fig. 3. It is seen that resistances in the 2nd and 4th cases gradually decrease and reach breakdown voltages at ~ 7.5 V and ~ 15 V, respectively. This means that when ESD discharges from $R-$ to $R+$, in the 2nd case, and $R-$ to ground, in the 4th case, the extrinsic breakdown plays an important role in explaining this phenomenon. On the contrast, intrinsic breakdown may elucidate the failed head characteristics of the 1st and 3rd cases where the ESD discharge is applied from $R+$ to $R-$ and $R+$ to ground, respectively. It can be seen that the resistances in both cases abruptly drops at ~ 9 V for the 1st case and ~ 30 V for the 4th case. In addition, it is observed in Fig. 1 that the impedance of the 3rd case is the largest and so, the head is rarely affected by the ESD discharge. Therefore, it needs the largest ESD voltage to cause the head the head to breakdown.

However, the extrinsic breakdown characteristic of the 1st and 3rd cases can also be observed under breakdown voltage or in a portion of initial breakdown, as shown in Fig. 4. In the 1st case, a gradual change of resistance is observed when an ESD voltage in the range of ~ 5 – 8 V is applied. It suddenly falls at ~ 8 V and steeply jumps at ~ 8.5 V. This remarkable effect of the 3rd case is observed at larger ESD discharging voltages. It is noticed that the resistance increases gradually for an ESD voltage range of ~ 27 – 28 V and then falls when the ESD voltage is higher than 28 V. These results show that the power dissipation generated by the ESD voltage can possibly affect the TMR head prior to electric field stress on the TMR head.

In order to understand the influence of discharge path on breakdown characteristic, an equivalent circuit derived from the head is used to analyze this breakdown characteristic. The voltage waveform across TMR for each case when the ESD voltage is of the order of 30 V is applied is shown in Fig. 5. The peak voltages and decay times of these consecutive ESD discharge cases are shown in Table 1. It is noticed that the peak voltages of the 1st and 2nd cases are similar whereas those of the other cases are at a much lower level. Although decay times of the 1st and 2nd cases show similar measurements, those of the 3rd and 4th cases differ.

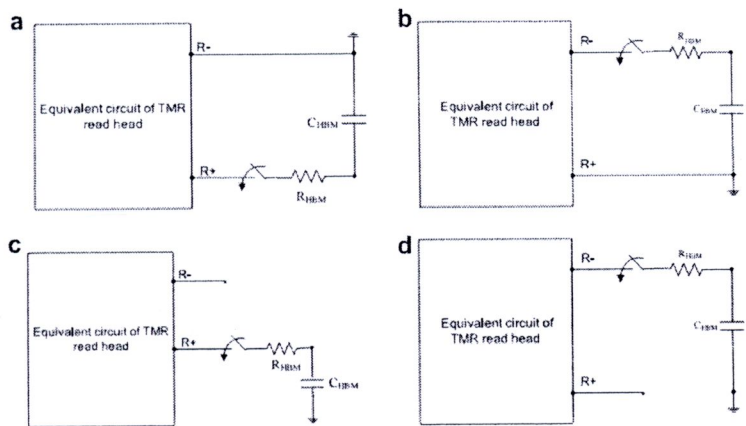


Fig. 2. Schematic diagrams of discharge in (a) 1st case = R- to R+, (b) 2nd case = R- to R-, (c) 3rd case = R- to ground and (d) 4th case = R+ to ground, where the box represents the equivalent circuit as shown in Fig. 1.

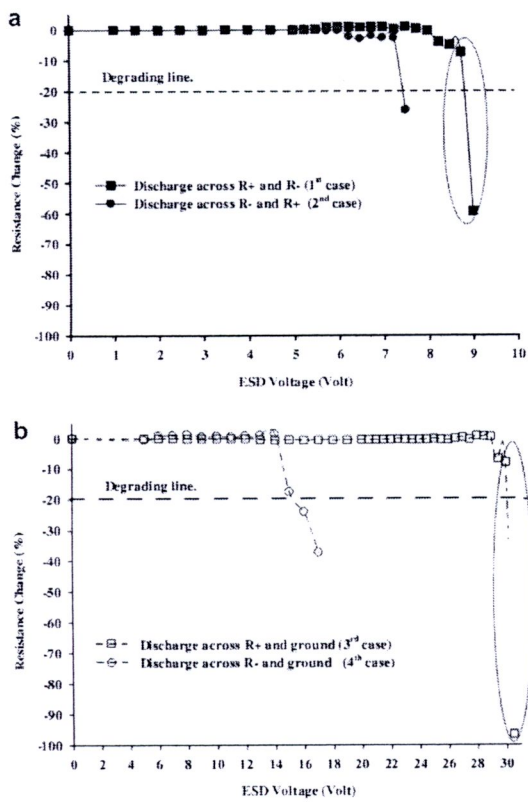


Fig. 3. Dependence of ESD voltage on resistance change. The line in the circle shows an abrupt change in resistance. a) Dependence of ESD voltage on resistance change at 1st and 2nd cases. b) Dependence of ESD voltage on resistance change at 3rd and 4th cases.

The inset shows a totally different waveform of substrate voltage. For example, peak voltages are high in the 3rd and 4th cases but low in the 1st and 2nd cases. This is possibly due to the current directly passing between R+ and R- without a leak to ground or passing a capacitance, in the 1st and 2nd cases, and so the decay time is long.

When considering the TMR voltage waveforms in Fig. 5, a possible reason to explain the difference in peak voltages between the 1st and 2nd cases, and the 3rd and 4th cases, is that the dissipative energy rarely passes the BS (Bottom Shield) and substrate elements for the 2 former cases. In addition, since the summarized R and C of the former cases are less than those of latter cases, the decay times of the 1st and 2nd cases are therefore longer.

On the contrary, the substrate voltage waveforms in the inset of Fig. 5 show large peak voltages for the 3rd and 4th cases. This can possibly be attributed to stored energy flowing through BS and substrate elements. The peak voltages are therefore large. In the 1st and 2nd cases, dissipative energy induced by ESD discharge hardly passes the substrate element and so, the substrate voltages are

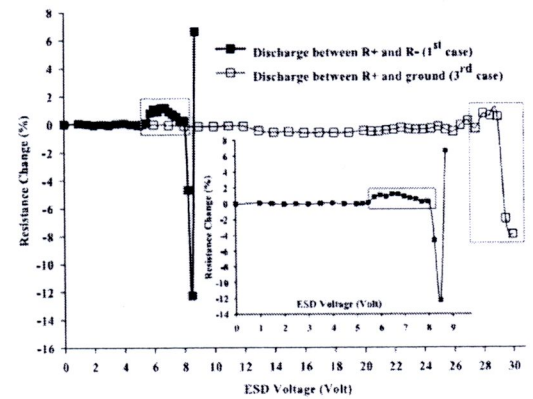


Fig. 4. Initial breakdown behavior observed in the 1st and 3rd cases where the inset shows initial breakdown characteristic for the 1st case and the box shows gradual changes in resistance.

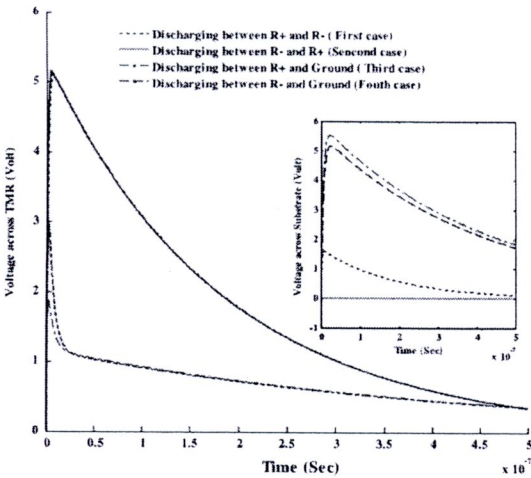


Fig. 5. Voltage waveforms of TMR sensor at an ESD voltage = 30 V where the inset shows waveforms of voltage across the substrate (C_Substrate).

smaller. In particular, when discharging from R– to R+ for the 2nd case, no leak energy dissipates to substrate element and so, the substrate voltage is nil. However, when discharging from R+ to R– in the 1st case, a divided voltage on the substrate element causes a small peak voltage. The dissimilar decay times are also explainable similarly to those of the TMR waveforms.

The differences may lead to an explanation of intrinsic and extrinsic breakdown of a TMR head as shown in Figs. 3 and 4. Since the energy is stored in BS and substrate elements, for discharging as in the 1st case, a lower dissipative energy on TMR is required. The resistance is then gradually changed at a lower ESD voltage. When the dissipative energy stored in BS and substrate elements abruptly discharges, an intrinsic breakdown is then seen in the 1st case.

For the 2nd case, the dissipative energy flowing through TMR without energy leakage on substrate element possibly generates pinholes inside the barrier insulator of the TMR. This therefore, causes an extrinsic breakdown.

For breakdown characteristics of the 3rd and 4th cases, it is seen in the inset of Fig. 5 that their substrate waveforms are alike. This may imply that stored energy of the substrate is insufficiently large to accelerate dielectric breakdown. In addition, the impedances of these cases are large and so a high activating energy is required to induce dielectric breakdown. Therefore, breakdown voltages of these cases are higher than those of the other cases. The characteristics of intrinsic and extrinsic breakdowns of the 3rd and 4th cases are explainable similarly.

3.2. Dependence of discharging path on waveform asymmetry

Discharging at different paths does not only affect head breakdown of TMR resistance but also of waveform asymmetry. It is clearly seen in Fig. 6 that discharging from R+ at first for both the

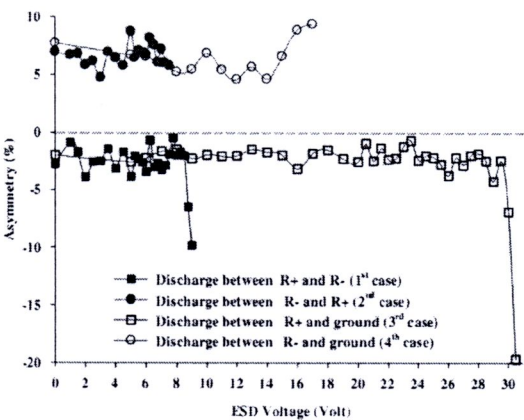


Fig. 6. Dependence of ESD voltage on TMR waveform asymmetry.

1st and 3rd cases, the waveform asymmetries are in the negative region. In contrast, when discharging from R– at first, positive signs of waveform asymmetry are observed.

This clearly proves the assumption that the asymmetric TMR circuit is totally different to the symmetric GMR circuit. For the 1st and 3rd cases, a positive biasing of TMR from BS to top-shield (TS) elements is thought to cause a negative result but for the 2nd and 4th cases a negative breakdown from TS to BS possibly causes a positive one. This may be attributed to the result of an asymmetric barrier inside the TMR sensor [11].

4. Conclusion

The breakdown characteristic of TMR read head when discharging at different path is investigated. The discharge from R+ at first can cause an intrinsic breakdown with negative waveform asymmetry whereas discharge from R– at first shows an extrinsic breakdown with positive waveform asymmetry. The proposed TMR equivalent circuit is sufficient to understand the breakdown mechanism. In the case of ESD stress by short circuit tests of the 1st and 2nd cases, the energy stored in substrate is explainable but for open circuit test of the 3rd and 4th cases, joule heating is the main reason considered.

Acknowledgment

This research is funded by the Industry/University Cooperative Research Center in HDD Components, Khon Kaen University, and the National Electronics and Computer Technology Center (NECTEC) under the National Sciences and Technology Development Agency (NSTDA), Thailand, Grant No. CPN-HR-03-01-50 D. The Authors would like to dedicate this work to staff of Western Digital (BangPa-In), Thailand, for their provision of samples, facilities and technical discussion, and thanks also to Ian Thomas, Department of Physics, Khon Kaen University, for the English proof.

References

[1] S. Mao, et al., Commercial TMR head for hard disk drives: characteristic and extendibility beyond 300 Gbit/inch², IEEE Trans. Magn. 42 (2006) 97–102.
[2] T. Kagami, et al., A performance study of next generation's TMR heads beyond 200 Gbit/inch², IEEE Trans. Magn. 42 (2) (2006) 93–96.

ARTICLE IN PRESS

N. Jutong et al. / Journal of Electrostatics xxx (2010) 1–5

5

- [3] K.Z. Gao, O. Heinonen, Y. Chen, Read and write processes, and head technology for perpendicular recording, *J. Magn. Mag. Mater.* 321 (6) (2008) 495–507.
- [4] F. Liu, C.H. Chang, J. Chen, B.B. Pant, Characteristic of electrostatic discharge induced damage on magnetic recording head, *IEEE Trans. Magn.* 42 (10) (2006) 2447–2449.
- [5] D. Guarisco, Resilience of tunneling magnetoresistive heads against electrical overstress, *J. Appl. Phys.* 103 (2008) p. 07F353.
- [6] A.W.Y. Lai, E.C.W. Leung, P.K. Wong, T. Shimizu, T. Kagami, M. Dovek, D. Hu, Anti-static robustness enhancement and high-frequency noise pickup immunity by internal shunting for tunneling magnetoresistive sensors, *IEEE Trans. Magn.* 44 (1) (2008) 104–106.
- [7] N. Jutong, D. Sompongse, P. Rakpongsiri, A. Siritariwat, Dependence of flex on suspension capacitance on human-boy-model-electrostatic-discharge affect TMR head, *Solid State Phenom.* 152–153 (2009) 439–442.
- [8] N. Jutong, D. Sompongse, P. Rakpongsiri, A. Siritariwat, Electrostatic discharge effect on TMR recording head: a flex on suspension capacitance Approach, *Int. J. Mod. Phys. B* 23 (17) (2009) 3586–3590.
- [9] B. Oliver, G. Tuttle, Q. He, X. Tang, J. Nowak, Two breakdown mechanisms in ultra thin alumina barrier magnetic tunnel junctions, *J. Appl. Phys.* 95 (3) (2004) 1315–1322.
- [10] S. Bae, J.H. Judy, I.-F. Tsu, M. Davis, Electrical reliability of tunneling magnetoresistive read heads, *J. Appl. Phys.* 94 (12) (2003) 7636–7645.
- [11] A. Arif Khan, J. Schmalhorst, A. Thomas, O. Schebaum, G. Reiss, Dielectric breakdown in Co–Fe–B/MgO/Co–Fe–B magnetic tunnel junction, *J. Appl. Phys.* 103 (2008) 123705-1–123705-5.
- [12] H. Xi, S. Franzen, J.I. Guzman, S. Mao, Degradation of magnetic tunneling junction cause by pinhole formation and growth, *J. Magn. Mag. Mater.* 319 (2007) 60–63.



ประวัติผู้เขียน

นายณัฐชัย จุทอง เกิดเมื่อวันที่ 15 ธันวาคม พ.ศ. 2520 ที่จังหวัดเพชรบูรณ์ จบการศึกษาระดับปริญญาตรี วิศวกรรมศาสตรบัณฑิต สาขาวิศวกรรมไฟฟ้า จากภาควิชาวิศวกรรมไฟฟ้า คณะวิศวกรรมศาสตร์ มหาวิทยาลัยรังสิต ในปี พ.ศ. 2543 ผู้เขียนได้เข้าศึกษาในระดับปริญญาโท สาขาวิศวกรรมไฟฟ้า มหาวิทยาลัยขอนแก่นในปี พ.ศ. 2543 และสำเร็จการศึกษาระดับมหาบัณฑิต สาขาวิศวกรรมไฟฟ้า เมื่อปี พ.ศ. 2546 โดยได้ทำการศึกษาเกี่ยวกับผลกระทบของการคายประจุไฟฟ้าสถิตในกระบวนการตัดสายขนาน

ในปี พ.ศ. 2548 จนถึงปัจจุบัน ผู้เขียนได้เข้าศึกษาต่อในระดับปริญญาเอก ปริญญาปรัชญาดุษฎีบัณฑิต สาขาวิศวกรรมไฟฟ้า มหาวิทยาลัยขอนแก่น

ประวัติการทำงาน

อาจารย์ประจำภาควิชาวิศวกรรมไฟฟ้า คณะวิศวกรรมศาสตร์ มหาวิทยาลัยรังสิต ระหว่างปี 2547-2548

